Journal of Alloys and Compounds 645 (2015) 57–63

Contents lists available at ScienceDirect

Journal of Alloys and Compounds

journal homepage: www.elsevier.com/locate/jalcom

Luminescence properties of nanocrystalline europium titanate $Eu_2Ti_2O_7$

Jan Mrázek [a,*], Martin Surýnek [a], Snejana Bakardjieva [b], Jiří Buršík [c], Jana Proboštová [a], Ivan Kašík [a]

[a] Institute of Photonics and Electronics AS CR, v.v.i., Chaberská 57, 18251 Prague 8, Czech Republic
[b] Institute of Inorganic Chemistry AS CR, v.v.i., 25068 Řež, Czech Republic
[c] Institute of Physics of Materials AS CR, v.v.i., Žižkova 22, 616 62 Brno, Czech Republic

ARTICLE INFO

Article history:
Received 16 January 2015
Received in revised form 3 April 2015
Accepted 4 May 2015
Available online 9 May 2015

Keywords:
Nanostructured materials
Luminescence
Europium
Pyrochlore

ABSTRACT

Nanocrystalline europium titanate $Eu_2Ti_2O_7$ with tailored structural properties was prepared by a sol–gel approach. Structural properties of prepared nanocrystals were correlated to the steady-state and time-resolved luminescence spectroscopy of europium ions incorporated within formed nanocrystals. The formation of nanocrystalline $Eu_2Ti_2O_7$ raised up the existence of two inequivalent positions of Eu^{3+} ions. Eu^{3+} ions displaced in highly symmetrical positions within the pyrochlore lattice provided low intensity luminescence and lifetime shorter than 10 μs. Eu^{3+} ions displaced in asymmetrical positions on the surface of formed nanoparticles provided lifetimes on the level of 50 μs. Number of Eu^{3+} ions displaced in asymmetrical positions was decreased according to increase size and crystallinity of formed nanocrystals. The presented results provide fundamental information about the influence of the structure and the morphology of formed nanocrystals to their luminescence properties.

1. Introduction

Europium-titanate $Eu_2Ti_2O_7$ belongs to the family of lanthanide titanates which crystallize in the pyrochlore crystal structure with the general formula $A_2B_2O_7$ [1]. The pyrochlores have attracted extensive attention of recent material research due to their phenomenal chemical and physical properties. In the pyrochlore structure, the sites of A-cations are occupied by ions of rare-earth elements (REE), the sites of B-cations are occupied by titanic ions [2]. The spins of atoms at A and B sites are arranged on the vertices of corner sharing tetrahedrons. These tetrahedrons are linked together into an infinite three-dimensional network allowing strong spin interactions within the lattice. Such an arrangement brings variety of magnetic properties that strongly depend on the REE incorporated within the pyrochlore crystal lattice [3]. For instance, spin-ice behavior was observed in case of Dy or Ho ions [4,5], anti-ferromagnetic ordering was observed for Er or Gd [6,7], ferroelectric properties were observed for La or La–Nd [8] alloyed phases, etc.

Although most of introduced rare-earth elements have been extensively exploited as constituents of inorganic phosphors, the pure $REE_2Ti_2O_7$ pyrochlores are optically inactive. The reason lies in the local site symmetry of REE arranged within the pyrochlore lattice. The pyrochlores belongs to the space group Fd3m (n°227) which is centrosymmetric. In this case all electric-dipole transitions between f–f orbitals, which are responsible for the luminescence of REE in visible and near infrared spectral region, are forbidden according to the Laporte selection rule [3]. However, if the local site symmetry of REE within the lattice is disturbed, the Laporte selection rule will not be fulfilled and the REE would appear luminescence properties. Generally speaking, any defects in the pyrochlore crystal lattice that decrease the local site symmetry of the incorporated REE would improve its luminescence properties. By reason that the real materials contain number of defects a very weak luminescence can be observed even in the case of the pyrochlore structure. Such a phenomenon was already demonstrated on a low-temperature luminescence of polycrystalline $Eu_2Ti_2O_7$ [9].

In our previous work; that was focused to the crystallization mechanism; we have reported a versatile sol–gel synthesis of nanocrystalline europium-titanate $Eu_2Ti_2O_7$ with tailored structural properties. Highly uniform nanocrystalline xerogels with tailored nanoparticle size were prepared by the sol–gel approach followed by the calcination of prepared gel. Thermal evolution of formed nanocrystals was followed by conventional structural methods; such as X-ray diffraction.

In this contribution, we report how the luminescence properties of nanocrystalline europium-titanate $Eu_2Ti_2O_7$ depend on the size and on the structure of prepared nanocrystals. Luminescence properties of europium ions incorporated within prepared nanocrystals were analyzed by steady-state and time-resolved luminescence

* Corresponding author. Tel.: +420 266 773 558; fax: +420 284 680 222.
E-mail address: mrazek@ufe.cz (J. Mrázek).

http://dx.doi.org/10.1016/j.jallcom.2015.05.019
0925-8388/

spectroscopy. Luminesce properties are related to the structural properties of formed nanocrystal. The presented results provide fundamental information about the influence of the structure and the morphology of formed nanocrystals to their luminescence properties.

2. Experimental

2.1. Materials and sample preparation

Samples were prepared by the sol–gel method followed by the thermal treatment of formed gel according to the presented approach [10]. Typically, a total of 6 g titanium(IV)butoxide (Fluka, Purum) was dissolved in 250 ml of absolute ethanol (Sigma–Aldrich, Spectranal grade). Then a total of 7.89 g of europium(III) nitrate hexahydrate was suspended in the solution. All precursors were used as purchased without further purification. The mixture was stirred under ambient temperature to form transparent solution. Formed solution was refluxed at 86 °C for 24 h and then allowed to cool. The solution was purified by a filtration through a 0.4 μm PTFE membrane and dried on a rotary evaporator. The resulting gel was pulverized and pre-calcined at 400 °C for 30 min with the heating rate 5 °C min^{-1} to burn-out volatile organic compounds. Finally, the fractions of pre-calcined xerogel were calcined to temperatures between 800 °C and 1200 °C for 30 min. Heating rate during the calcination was 10 °C min^{-1}. The calcinations were carried out under a 10 l min^{-1} flow of oxygen.

2.2. Characterization techniques

Transmission electron microscopy (TEM) analyses of the analyzed xerogels were carried out on Philips CM12 STEM electron microscope. High-resolution transmission electron microscopy (HRTEM) imaging was carried out using a JEOL JEM 3010 electron microscope operating at 300 kV (LaB_6 cathode) with a point resolution of 1.7 Å. For both analyzes, a copper grid coated with a porous carbon support film was used as a sample holder. The sample xerogel was dispersed in ethanol, and the resulting suspension was treated in an ultrasonic bath for 10 min and then applied to the grid.

The luminescence spectra were recorded on a Fluorolog 3 (Horiba Jobin–Yvon) spectrometer equipped with a photomultiplier and a single-photon counting module (IBH datastation). A high-pass optical filter Schott KV 550 with an edge at 550 nm was placed at the input of emission monochromator to fully suppress a stray-light and to improve the quality of detected signal. All samples were analyzed in a reflection set-up.

Steady-state luminescence was excited by 450 W xenon lamp. The excitation spectra were recorded from 350 to 550 nm with a step 1 nm and a slit 1 nm. The emission spectra were recorded from 570 to 720 nm with a step 0.5 nm and a slit 1 nm. The emission spectra of selected xerogels were recorded in the range from 400 to 800 nm without the high-pass filter to proof the lack of presence of Eu^{2+} in the calcined samples. The integration time was 0.5 s for all steady-state measurements.

Time-resolved luminescence was excited by a laser diode (LD) module (Top-GaN) emitting at 405 nm with an optical power 50 mW. The laser diode was synchronized with the single-photon counting module operating in a master mode. Time-resolved emission was recorded at a wavelength 610 nm with a 3 nm emission slit. Histogram with a maximum frequency 100,000 counts was recorded for each sample. Recorded data were correlated to the signal delay of the laser diode and further analyzed in Origin 8 software. Then the experimental data were fitted by the linear combination of two exponential decay curve. The fits were expressed by the equation:

$$I_L = A_1 \cdot e^{\frac{-t}{\tau_1}} + A_2 \cdot e^{\frac{-t}{\tau_2}}, \quad (1)$$

where I_L represents the time-resolved luminescence intensity, t is the time, τ_1 and τ_2 luminescence lifetimes, A_1 and A_2 amplitudes. The amplitudes represent the contribution of particular exponential curves to the overall luminescence intensity I_L. If one amplitude is equal to zero then the two exponential decay curve pass into a single exponential decay curve.

3. Results and discussion

3.1. Thermal behavior and structural evolution of xerogels

In our previous work [10] we have demonstrated the thermal behavior and structural evolution of nanocrystalline europium-titanate $Eu_2Ti_2O_7$ prepared by the sol–gel approach. It has been concluded that the crystallization is limited by the presence of nitrates which are burn-out at temperatures above 800 °C. The crystallization started between 800 and 850 °C. The crystallization process consists by the homogenous nucleation followed by the three dimensional growth of formed nanocrystals.

Highly pure nanocrystalline $Eu_2Ti_2O_7$ was prepared by the sol–gel method followed by the calcination. Chemical analysis of xerogels confirmed the chemical formula $Eu_{2.06}Ti_2O_{7.09}$. The approach resulted into the formation of nanocrystals with tailored grain size and crystallinity. The calculated mean grain size and the crystallinity of calcined xerogels regularly grew up with increasing temperature as is summarized in Fig. 1.

3.2. Structural properties of formed nanocrystals

The structure of analyzed xerogels was proved by TEM measurements that are depicted in Fig. 2. The primary nanocrystals formed at 850 °C were agglomerated into irregular grains with the size ranging from 50 to several hundreds of nanometers. The nanocrystals were randomly distributed within the amorphous matrix as was confirmed by the diffraction pattern depicted in Fig. 2b. This structure explains why the xerogel calcined at 850 °C was very soft and mechanically adjustable. TEM imaging, demonstrated in Fig. 2c, showed that the xerogel calcined at 1100 °C was composed by clearly limited grains with broad grain size distribution ranging from 50 to 130 nm. However, the calculated nanocrystal size was around 76 nm. This discrepancy is completely natural, because the calculated size express the mean value of size distribution. Diffraction patterns of individual grain depicted in Fig. 2e and f, confirmed that the grain was identical to formed nanocrystal. The diffractions patterns measured on the particular grains corresponded to the face-centered cubic lattice with the lattice parameter a = 1.02 nm. This value well matched the value 1.0193 nm given by the JCPDS database for $Eu_2Ti_2O_7$.

The validity of using xerogels thermally calcined at 1200 °C as the reference for the calculation of the crystallinity was proved by HRTEM analysis depicted in Fig. 3. Analyzed nanoparticles were clearly limited and their size ranged from 100 to 200 nm. Corresponding diffraction pattern, recorded on the agglomerate of nanoparticles, confirmed their random orientation. The xerogel was perfectly crystalline in the nanoscale without presence of larger defects. The evaluation of interplanar distances provided the lattice parameter a = 1,018 nm. This value perfectly match the value evaluated from TEM measurements.

3.3. Luminescence properties of xerogels

3.3.1. Luminescence properties of Eu^{3+} ions

The luminescence properties of rare earth elements doped materials have been frequently studied on the basis of the crystal

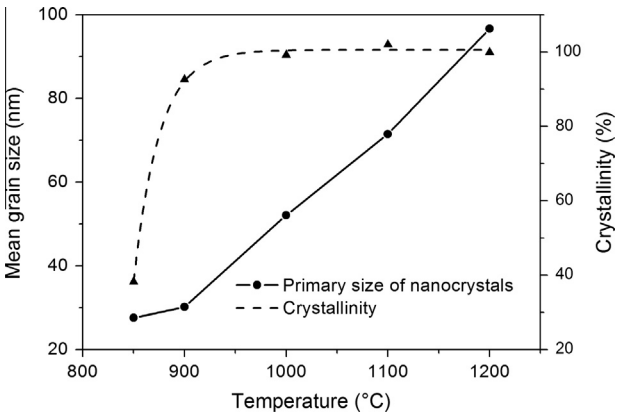

Fig. 1. Thermal evolution of the calculated nanocrystal mean size (left scale) and the crystallinity (right scale).